V European Conference on Computational Fluid Dynamics
ECCOMAS CFD 2010
J. C. F. Pereira and A. Sequeira (Eds)
Lisbon, Portugal,14-17 June 2010

SHARP INTERFACE SIMULATIONS OF SURFACTANT-COVERED DROPS IN ELECTRIC FIELDS

Knut Erik Teigen*, Karl Yngve Lervåg† and Svend Tollak Munkejord†

*Norwegian University of Science and Technology,
Department of Energy and Process Engineering
NO-7491 Trondheim, Norway
e-mail: knut.erik.teigen@ntnu.no, knutert@gmail.com

†SINTEF Energy Research, Energy Processes
NO-7465 Trondheim, Norway
e-mail: {karl.lervag,svend.t.munkejord}@sintef.no

Key words: fluid dynamics, multiphase flow, surfactant, level-set method, sharp interface, ghost-fluid method

Abstract. *A level-set method for computations of interfacial flows with insoluble surfactants with electric fields is presented. The discontinuities at the interface are captured in a sharp manner using the ghost-fluid method. The accuracy of the method is tested and compared to the standard level-set method. The method is then used to study the combined effect of insoluble surfactants and electric fields on the motion and deformation of a falling drop. It is found that the surfactant generally reduces the deformation and the terminal velocity of the drop. This reduction is most pronounced in the nearly spherical regime where the drop behavior is similar to a solid sphere due to the interface immobilization caused by the presence of a surfactant. The electric field increases the terminal velocity by stretching the drop in the direction of the electric field. This effect is largest for the surfactant-covered drop, which is deformed more due to the lower average interfacial tension.*

1 INTRODUCTION

The presence of surface-active agents (surfactants) at fluid interfaces can have a considerable effect on flow dynamics. Surfactants are amphiphilic organic compounds, which can be adsorbed at liquid-gas or liquid-liquid interfaces. The presence of surfactants typically alters the interface dynamics by a reduction in the interfacial tension. An inhomogeneous distribution of surfactants produces gradients in interfacial tension, which again gives rise to tangential forces along the interface. Through this so-called Marangoni effect, surfactants can play an important role in several physical phenomena, for instance vortex pair interaction[50,14], fingering[49,29] and drop break-up and coalescence[15,17,25,12].

The authors' interest is the influence of surfactants on the breaking of water-in-oil emulsions. In some oil fields, heavy oils with high viscosity combined with surface-active

components like asphaltenes and resins make it hard to extract the water using traditional sedimentation processes. In order to accelerate the sedimentation process, an electric field can be applied to the emulsion[8]. This will introduce attractive forces between the water drops, which increase the coalescence rate and thereby also the sedimentation rate.

Both the influence of surfactants and electric fields on drops have been studied numerically. However, to the authors' knowledge, this is the first numerical study of the combined effect of surfactant and electric fields. The available numerical methods for detailed simulations of two-phase flows can roughly be divided into two categories: interface-tracking and interface-capturing methods. Interface-tracking methods use either a separate grid for the interface, or a set of interconnected points to mark the interface. Examples of methods which have been applied to both surfactants and electric fields include the boundary-integral method[41,32,31,40,24] and the front-tracking method[19,56,34,16]. In general, interface-tracking approaches can be made very accurate, but can be relatively complicated to implement, especially in three dimensions and for problems involving topological changes.

In interface-capturing methods, the interface is not tracked explicitly, but instead is implicitly defined through a regularization of the interface. This means that the evolution of the interface is handled independently of the underlying grid, which greatly simplifies gridding, discretization and handling of topological changes. Well known methods in this category include the volume-of-fluid method[39,18], the phase-field method[46,47] and the level-set method[54,53,52,48,3]. Other novel methods are the lattice-Boltzmann method with electric fields[57] and the smoothed particle hydrodynamics method with soluble surfactants[2].

In this paper, we build upon the previous work of Xu et al. (2006)[53], and use the level-set method to represent the interface. However, instead of using the immersed-interface method[26] (IIM) to handle discontinuities across the interface, we employ the ghost-fluid method[9] (GFM). For the case of constant coefficients in the jump conditions, the GFM is a lower order version of the IIM. The main disadvantage of the IIM is that discontinuity relations for higher-order derivatives must be developed and implemented. For more complex physical systems, these may not be available *a priori*, in which case an iterative method has to be used to calculate the discontinuites, leading to a more complex implementation and a more expensive computation. The GFM has the advantages that it is more accurate than the standard level-set method based on a diffuse interface, the so-called continuous surface force (CSF) method, while remaining computationally efficient and relatively easy to implement for both two- and three-dimensional problems. A ghost-fluid method for electric fields was presented in Hansen (2008)[3], and we use the same methodology here.

The paper is organized as follows: In Section 2, we state the governing equations and briefly discuss the numerical method. In Section 3 we present simulations demonstrating the capabilities of the method. We first compare the accuracy to a diffuse-interface method using a test case with an available analytical solution, then we present simulations of a

falling drop and discuss the influence of surfactants and electric fields. Section 4 concludes the work.

2 GOVERNING EQUATIONS AND NUMERICAL METHODS

The full Navier–Stokes equations are solved in each phase, and the interface between the two phases is captured using the level-set method. The ghost-fluid method is used to treat discontinuities across the interface in a sharp manner.

2.1 Flow equations

The flow is governed by the incompressible Navier–Stokes equations, with added terms for interfacial-tension forces and electric forces:

$$\begin{aligned} \rho\left(\frac{\partial \boldsymbol{u}}{\partial t} + (\boldsymbol{u}\cdot\boldsymbol{\nabla})\boldsymbol{u}\right) &= -\boldsymbol{\nabla}p + \boldsymbol{\nabla}\cdot[\mu(\boldsymbol{\nabla}\boldsymbol{u} + \boldsymbol{\nabla}\boldsymbol{u}^T)] + \rho\boldsymbol{g} + \boldsymbol{F_e} + \boldsymbol{F_s}, \\ \boldsymbol{\nabla}\cdot\boldsymbol{u} &= 0. \end{aligned} \tag{1}$$

Here, ρ is the density, $\boldsymbol{u}$ is the velocity, p is the pressure, μ is the dynamic viscosity and $\boldsymbol{g}$ is the gravitational acceleration. F_e is the force due to the presence of an electric field. The effect of an interface, Γ, in the domain results in a singular interfacial force which can be expressed by

$$\boldsymbol{F_s}(\boldsymbol{x},t) = \int_{\Gamma(t)} \hat{\boldsymbol{F}}_{\boldsymbol{s}}(s,t)\delta(\boldsymbol{x} - \boldsymbol{X}(s,t))\mathrm{d}s, \tag{2}$$

where s is the arc-length, $\boldsymbol{X}(s,t)$ is the parametrization of the interface, $\boldsymbol{x}$ is the spatial position and δ is the Dirac delta function. For the present problem, $\hat{\boldsymbol{F}}_{\boldsymbol{s}}$ is given by

$$\hat{\boldsymbol{F}}_{\boldsymbol{s}} = \sigma\kappa\boldsymbol{n} - \boldsymbol{\nabla}_\Gamma\sigma \tag{3}$$

The first term accounts for the normal capillary force due to interfacial tension. Here, σ is the coefficient of interfacial tension, κ the curvature and $\boldsymbol{n}$ is the outward pointing unit normal vector. The second term is the Marangoni force, which is caused by gradients in the interfacial tension and acts tangentially to the interface. The interfacial gradient, $\boldsymbol{\nabla}_\Gamma$, is given by

$$\boldsymbol{\nabla}_\Gamma = (\boldsymbol{I} - \boldsymbol{n}\boldsymbol{n})\boldsymbol{\nabla}, \tag{4}$$

where $\boldsymbol{I}$ is the identity tensor.

2.2 Surfactants

Gradients in the interfacial tension occur due to the presence of an insoluble surfactant on the interface. The dynamics of the surfactant concentration, f, is governed by[54,53]

$$\begin{aligned} &\frac{\partial f}{\partial t} + \boldsymbol{u}\cdot\boldsymbol{\nabla}f - \boldsymbol{n}\cdot\boldsymbol{\nabla}\boldsymbol{u}\cdot\boldsymbol{n}f \\ &\quad = D_f\left(\boldsymbol{\nabla}^2 f - \boldsymbol{n}\cdot\boldsymbol{\nabla}\boldsymbol{\nabla}\cdot\boldsymbol{n}f + \kappa(\boldsymbol{n}\cdot\boldsymbol{\nabla}f)\right) \end{aligned} \tag{5}$$

where D_f is the surfactant diffusion coefficient. We employ the Langmuir equation of state to relate the interfacial tension and surfactant concentration,

$$\sigma(f) = \sigma_0 \left[1 + \beta \ln \left(1 - \frac{f}{f_\infty} \right) \right]. \tag{6}$$

Here, $\beta = \bar{R}T f_\infty / \sigma_0$ is the interface elasticity number, which is a measure of the sensitivity of interfacial tension to surfactant concentration. f_∞ is the maximum surfactant packing, $\bar{R}$ is the universal gas constant, T the temperature and σ_0 is the interfacial tension of a clean interface.

In this paper, we will assume that the surfactant is restricted to the interface, i.e. it will not be able to dissolve into the surrounding fluid. Surfactants behave as insoluble monolayers in two limits[37]. The first corresponds to dilute bulk concentrations, for which the diffusion flux from the bulk is slow compared to the interface convection flux. The second limit corresponds to slow adsorption-desorption exchange, which can occur in aqueous systems with long-chained surfactants.

Since we assume that the surfactant is insoluble, it is only defined on the interface. In order to solve the evolution equation numerically, we must therefore first extend the surfactant concentration off the interface[58]. This is accomplished by solving[1]

$$\frac{\partial f}{\partial \tau} + S(\phi_0) \boldsymbol{n} \cdot \boldsymbol{\nabla} f = 0. \tag{7}$$

Here, S is a sign function given by

$$S(\phi) = \frac{\phi}{\sqrt{\phi^2 + 2\Delta x^2}}. \tag{8}$$

Note that this equation is hyperbolic, so it is not necessary to solve it to steady state, since only the information a few grid points away from the interface is relevant.

2.3 Electric forces

We want to model a conductive drop in an otherwise dielectric medium, for instance a water drop in oil. This can be achieved by assuming perfect dielectric materials with no free charges, and then choosing a high permittivity ratio between the two phases[30].

With these assumptions, the electric force is given by

$$\boldsymbol{F}_e = \boldsymbol{\nabla} \cdot \boldsymbol{M}, \tag{9}$$

where $\boldsymbol{M}$ is the Maxwell stress tensor,

$$\boldsymbol{M} = \varepsilon \varepsilon_0 \left[\boldsymbol{E}\boldsymbol{E} - \frac{1}{2} (\boldsymbol{E} \cdot \boldsymbol{E}) \boldsymbol{I} \right]. \tag{10}$$

Here, $\boldsymbol{E}$ is the electric field. With the above assumptions, $\boldsymbol{\nabla\cdot M} = \boldsymbol{0}$ everywhere except at the interface. The electric field is divergence free, such that

$$\boldsymbol{E} = -\boldsymbol{\nabla}\Psi, \tag{11}$$

where Ψ is the electric potential. The electric potential is found from the following Laplace equation:

$$\boldsymbol{\nabla\cdot}(\varepsilon\varepsilon_0\boldsymbol{\nabla}\Psi) = 0. \tag{12}$$

2.4 Interface capturing

The interface is captured using the level-set method[44,36]. This method allows accurate computation of the evolution of an interface, along with automatic handling of topological changes. The ghost-fluid method[9,21] (GFM) is used to take discontinuities across the interface into account. This method handles the jumps in physical properties directly in the numerical stencils, without the need for any smearing of properties.

The GFM requires jump conditions, which are relations between the physical quantities on each side of the interface. The jump conditions for the present problem are[21,3,13]

$$[\boldsymbol{u}] = 0, \tag{13}$$

$$[p] = 2[\mu]\boldsymbol{n}\cdot\boldsymbol{\nabla u}\cdot\boldsymbol{n} + \boldsymbol{n}\cdot[\boldsymbol{M}]\cdot\boldsymbol{n} + \sigma\kappa, \tag{14}$$

$$[\Psi] = 0, \tag{15}$$

$$\begin{aligned}[\mu\boldsymbol{\nabla u}] = [\mu]\Big(&(\boldsymbol{n}\cdot\boldsymbol{\nabla u}\cdot\boldsymbol{n})\boldsymbol{nn} + (\boldsymbol{n}\cdot\boldsymbol{\nabla u}\cdot\boldsymbol{t})\boldsymbol{nt} \\ &- (\boldsymbol{n}\cdot\boldsymbol{\nabla u}\cdot\boldsymbol{t})\boldsymbol{tn} + (\boldsymbol{t}\cdot\boldsymbol{\nabla u}\cdot\boldsymbol{t})\boldsymbol{tt}\Big) \\ &- (\boldsymbol{t}\cdot[\boldsymbol{M}]\cdot\boldsymbol{n})\boldsymbol{tn} - (\boldsymbol{t}\cdot\boldsymbol{\nabla}_\Gamma\sigma)\boldsymbol{tn},\end{aligned} \tag{16}$$

$$[\boldsymbol{\nabla}p] = 0, \tag{17}$$

$$[\varepsilon\boldsymbol{n}\cdot\boldsymbol{\nabla}\Psi] = 0. \tag{18}$$

A well-known issue with the level-set method is that it does not conserve mass. The more accurate ghost-fluid discretization somewhat alleviates the problem, but for long-running simulations it is still an issue. In particular, since we use an explicit time-integration method in this work, simulations at low Reynolds numbers (i.e. highly viscous fluids) suffer from severe mass loss. We therefore introduce a simple mass correction scheme for these simulations. At each time step, we add a constant, α, to the level-set function, where α is found by solving the equation

$$\int_\Omega H(\phi)(\phi+\alpha)\mathrm{d}\Omega = \int_\Omega H(\phi_0)\phi_0\mathrm{d}\Omega. \tag{19}$$

Here, ϕ_0 is the initial level-set function. The effect of this correction scheme is to add any lost mass back globally over the entire drop. Since mass loss typically occurs in regions of high curvature and low resolution, this scheme works well for low Reynolds number

drops, which tend to remain nearly spherical. We note that more sophisticated approaches for dealing with the mass loss exist. These include coupling with Lagrangian particles[7], coupling with the VOF method[43,51] and using modified advection procedures[35,38,28].

2.5 Numerics

A second-order projection scheme is used to solve the Navier–Stokes equations. The evolution in time is performed using a four-step third-order, strong stability-preserving (SSP) Runge-Kutta (RK) method[23,22], while a second-order SSP RK method is employed for the evolution of the level-set equation, the reinitialization of the level-set equation and extrapolation of the velocity field and surfactant concentration.

The equations are spatially discretized on an equidistant staggered grid with cell spacing h, where scalar values are stored in cell centers and vector values are stored at cell boundaries. The convective terms are discretized using the fifth order Weighted Essentially Non-Oscillatory (WENO) scheme[20], and Laplacian and gradient terms are discretized using the ghost-fluid version of standard, second-order central differences. The Poisson equations for pressure and electric potential are solved using a multigrid algorithm.

To reduce the computational costs, we use a simple scheme to move the domain along with the falling drop. If the mass center of the drop moves to a neighboring grid cell, the grid is shifted one cell in the opposite direction to account for this, and data is extrapolated to the new grid cells.

3 RESULTS

In this Section, we present some numerical results on drop dynamics using the above method. We begin by validating the implementation of the Marangoni stresses by simulating a bubble rising due to thermocapillary effects. Here, we also compare the results to the CSF method. The implementation of electric forces has been validated and compared against the CSF method elsewhere[46]. Next, we investigate the influence of surfactants and electric fields on a viscous drop falling through a viscous medium, e.g. a water drop falling through oil. Two representative systems are studied, one at a low Reynolds number where the drop remains spherical, and one at a high Reynolds number where the drop deforms significantly.

3.1 Bubble rising due to thermocapillary effects

As a test case for the implementation of the interfacial-tension force, we will simulate the thermocapillary migration of a bubble. It is well known that due to the dependence of interfacial tension on temperature, there will be a discontinuity in the tangential stresses across the interface for a bubble in a temperature gradient[55]. The result is a motion of the drop in a direction that will reduce its interfacial free energy. The flow at the interface will be from the warmer to the cooler pole of the bubble, and therefore, the bubble will move

in the direction of the warmer pole. This motion is known as thermocapillary migration.

We assume that the temperature varies as

$$\frac{T(z)}{T_\infty} = \frac{z}{L}, \tag{20}$$

where L is the domain height, and the relationship between temperature and interfacial tension is

$$\sigma(z) = \sigma_0 \left(1 - \beta \frac{T(z)}{T_\infty}\right). \tag{21}$$

We assume that the pressure in the surrounding fluid is zero. Then the pressure inside the bubble is given by

$$p(z) = \frac{2\sigma(z)}{R}, \tag{22}$$

where R is the bubble radius. For a viscous bubble in a linear temperature gradient, an approximation for the terminal rise velocity is[55]

$$V_{YBG} = \frac{2\Big(\sigma_0 \beta R/L - \Delta\rho g R^2 (\mu_1 + \mu_2)/\mu_2\Big)}{(6\mu_1 + 9\mu_2)}. \tag{23}$$

Here, we choose a domain size $5R \times 15R$, and parameters $\mu_1 = \mu_2 = 0.2\,\mathrm{Pa,s}$, $R = 0.5\,\mathrm{m}$, $\sigma_0 = 1.0\,\mathrm{N/m}$ and $\beta = 1.0$. Gravity effects are neglected. According to Eq. (23), this should give a Reynolds number of $\mathrm{Re} = 0.0444$, which is well within the creeping flow regime for which the equation is valid.

We first compare the GFM and the CSF method with respect to Eq. (22) for the pressure. Fig. 1a shows a close-up of pressure contours inside the bubble. In Fig. 1b, the pressure along the vertical center line is compared to the analytical result for both the GFM and the CSF method for $R/h = 10$. We see that with the GFM, the jump in pressure at the interface is treated in a sharp manner, and that the pressure inside the bubble is accurately captured. For the CSF, however, the discontinuity is smeared out, and the jump in pressure is over-predicted. In Table 1, the relative error of the pressure in the bubble center is given together with convergence rates for the GFM. The error decreases in a first-order fashion, which is consistent with other results obtained with the GFM[3].

Next, we compare the simulated rise velocity to Eq. (23). The computational rise velocity was calculated with

$$V(t) = \frac{\int_\Omega H(\boldsymbol{x}, t)\boldsymbol{u}(\boldsymbol{x}, t) \cdot \boldsymbol{e}_z \mathrm{d}\Omega}{\int_\Omega H(\boldsymbol{x}, t)\mathrm{d}\Omega}, \tag{24}$$

where $H(\boldsymbol{x}, t)$ is the smeared out Heaviside function and $\boldsymbol{e}_z$ is the unit vector in the z-direction. This integral was evaluated using the midpoint rule.

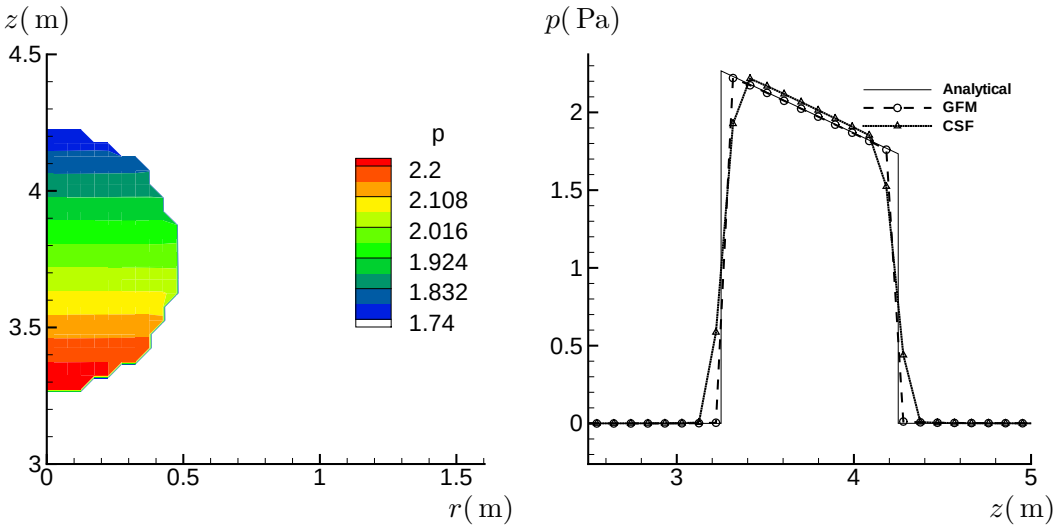

(a) Pressure contours after one time step.

(b) Pressure along vertical centerline compared to analytical result, Eq. (22).

Figure 1: Pressure after one time step for a bubble rising in a linear surfactant gradient.

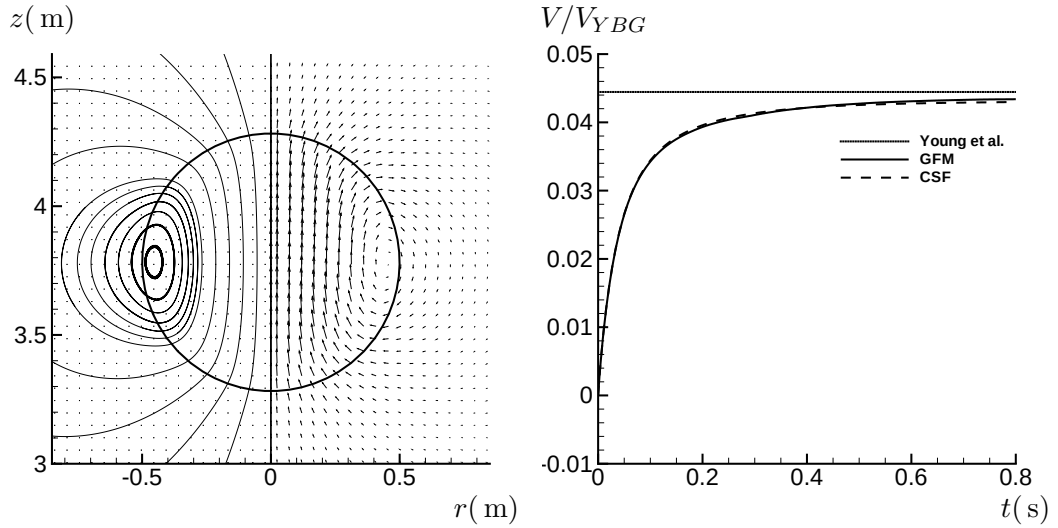

(a) Velocity vectors at steady state.

(b) Rise velocity compared to theoretical result.

Figure 2: Velocity field at steady state and rise velocity versus time for the thermocapillary migration test case.

Table 1: Thermocapillary migration test case. Error and convergence for the pressure inside the bubble after one time step.

R/h	Relative error ($\times 10^{-2}$)	Order
10	1.28	–
20	0.655	0.97
30	0.330	0.99
40	0.168	0.98

Table 2: Parameters for falling drop at low Reynolds number

Parameter	Symbol	Value
Drop radius	R	$1.03 \times 10^{-3}\,\mathrm{m}$
Drop density	ρ_1	$1.128 \times 10^{3}\,\mathrm{kg/m^3}$
Matrix density	ρ_2	$9.49 \times 10^{2}\,\mathrm{kg/m^3}$
Drop viscosity	μ_1	$6.3 \times 10^{-3}\,\mathrm{Pa\,s}$
Matrix viscosity	μ_2	$3.8 \times 10^{-2}\,\mathrm{Pa\,s}$
Interfacial tension	σ	$2.91 \times 10^{-3}\,\mathrm{N/m}$
Surfactant concentration	f_0	$2.4 \times 10^{-6}\,\mathrm{mol/m^2}$
Maximum surfactant packing	f_∞	$6.0 \times 10^{-6}\,\mathrm{mol/m^2}$
Interface elasticity	β	0.4
Diffusion coefficient	D_f	$1 \times 10^{-6}\,\mathrm{m^2/s}$
Electric field	E_0	$8 \times 10^{5}\,\mathrm{V/m}$
Drop relative permittivity	ε_1	250
Matrix relative permittivity	ε_2	1

The velocity field around the bubble at steady state is shown in Fig. 2a for a grid spacing of $R/h = 10$. The figure is in good agreement with results from the literature[34]. Fig. 2b shows the normalized rise velocity for both the GFM and the CSF method. After an initial acceleration phase, the velocity approaches the theoretical prediction asymptotically. We observe that the results for the GFM is closer to the theoretical value. However, the accuracy is surprisingly good for both methods considering the relatively coarse grid used. For the GFM, the difference between the theoretical rise velocity and the computed at $t = 0.8\,\mathrm{s}$ is 2.38%, while for the CSF method, the difference is 3.31%.

3.2 Falling drop at low Reynolds number

We now consider a drop falling in a gravity field at a low Reynolds number. The parameters chosen are given in Table 2. In terms of dimensionless numbers, these pa-

rameters give an Eötvös number of $\mathrm{Eo} = \Delta\rho g D^2/\sigma = 0.256$ and a Morton number of $\mathrm{Mo} = \Delta\rho g\mu_2^4/\rho_2^2\sigma^3 = 1.65 \times 10^{-4}$. For these low values, the drop moves slowly with a nearly spherical shape[4].

At low Reynolds numbers, we can compare our numerical results to the Hadamard-Rybczynski formula for a viscous drop in creeping flow[11],

$$V_{T,\mathrm{HR}} \frac{2\Delta\rho g R^2(\mu_1 + \mu_2)}{3\mu_2(3\mu_1 + 2\mu_2)}. \tag{25}$$

For the parameters considered here, we get $V_{T,\mathrm{HR}} = 1.53 \times 10^{-2}\,\mathrm{m/s}$, or $\mathrm{Re} = 0.785$.

For the simulations, we choose a domain size of $16R \times 32R$ and a grid spacing of $R/h = 20$. The simulated terminal velocity is $V_T = 1.40 \times 10^{-2}\,\mathrm{m/s}$, which is close to the predicted value. The discrepancy is most likely due to the simulation being performed in a bounded domain, as opposed to the formula which is derived for an infinite domain.

Next, we look at the effect of having a surfactant on the interface. For the contaminated drop, the simulated terminal velocity is reduced to $V_T = 0.96 \times 10^{-2}\,\mathrm{m/s}$. The reason for this becomes evident by looking at the velocity profiles given in Figure 3. For the contaminated drop, the internal circulation nearly disappears, and the drop behaves close to a rigid particle. The Stokes formula for a rigid, spherical particle in creeping flow,

$$V_{T,\mathrm{S}} \frac{2\Delta\rho g R^2}{9\mu_2}, \tag{26}$$

gives $V_{T,\mathrm{S}} = 1.09 \times 10^{-2}\,\mathrm{m/s}$, which is close to the terminal velocity for the contaminated drop. Again, the discrepancy is attributed to the bounded domain.

Figure 4a shows the surfactant concentration as a function of the arc length, s, measured in the counter-clockwise direction. The surfactant concentration takes the shape of an S-curve, and hence the Marangoni stresses are evenly distributed across the drop. The consequence of this is illustrated in Figure 4b, which shows the interface velocity for both the clean and the contaminated drop. The interface velocity of the contaminated drop is greatly reduced across the entire drop interface.

We then consider the effect of an electric field. The drop is allowed to reach a steady state before the electric field is switched on. The strength of the electric field can be characterized by the electric capillary number, $\mathrm{Ca}_E = \varepsilon_0\varepsilon_2 D E_0^2/\sigma$. A conductive drop submitted to an electric field becomes unstable when $\mathrm{Ca}_E \approx 0.41$[45]. However, here the gravitational force will act to stabilize the drop, allowing the use of an even higher Ca_E. We choose $\mathrm{Ca}_E = 0.45$, which gives $E_0 \approx 8 \times 10^5\,\mathrm{V/m}$.

Figure 5a illustrates the drop shape for the clean drop, along with electric field lines and velocity vectors. The drop clearly stretches into a prolate shape. This more streamlined profile gives a reduction in drag and hence a higher terminal velocity. The terminal velocity was calculated to be $V_T = 1.50 \times 10^{-2}\,\mathrm{m/s}$, an increase over the clean drop without an electric field. The aspect ratio of the drop is 0.770, while theory predicts

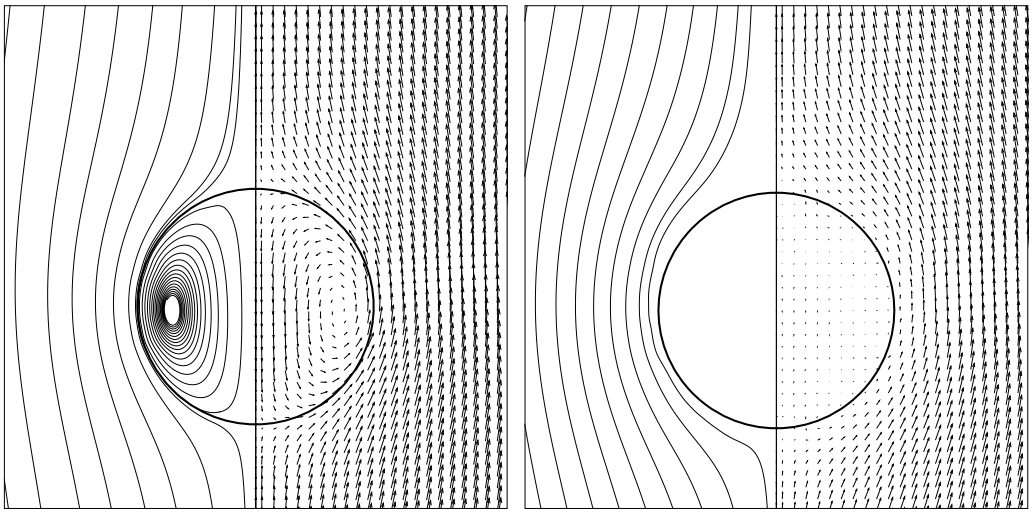

(a) Clean (b) Contaminated

Figure 3: Low Re drop. Streamlines and velocity vectors in a coordinate system moving with the drop centroid. Velocity vectors are plotted at every other grid point.

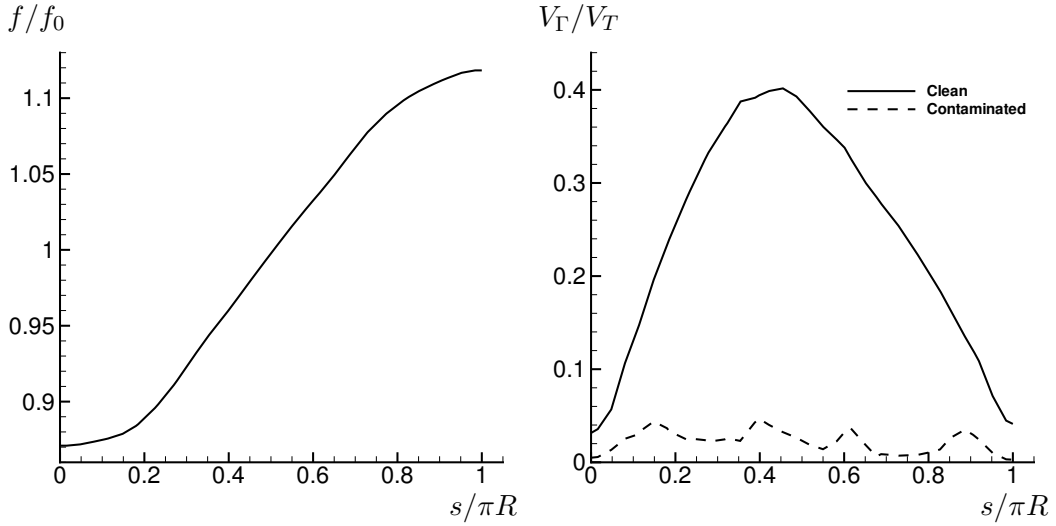

(a) Surfactant concentration (b) Interface velocities

Figure 4: Low Re drop. Surfactant concentration and interface velocities as functions of arc length.

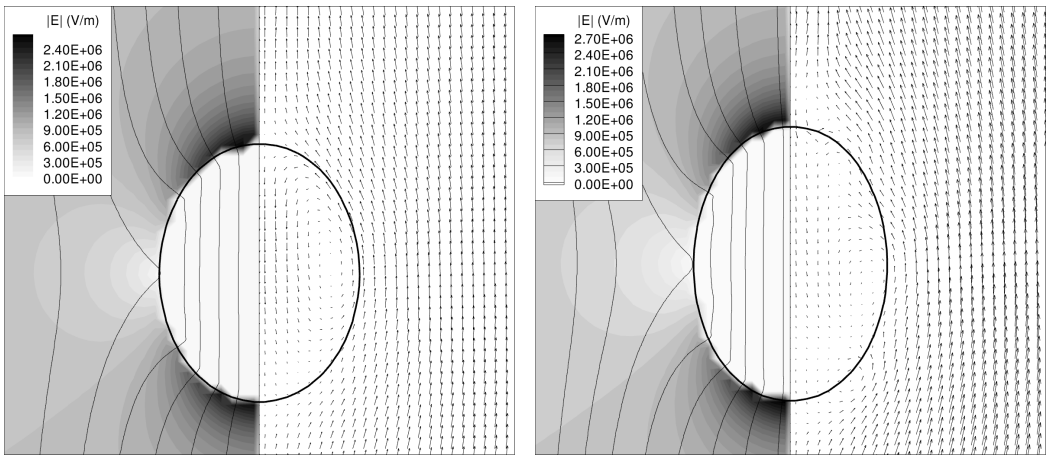

(a) Clean (b) Contaminated

Figure 5: Low Re drop with electric field. The left part of the drop shows streamlines of the electric field and contours colored by the electric field magnitude. The right part of the drop shows velocity vectors in a coordinate system moving with the drop centroid. Velocity vectors are plotted at every other grid point.

a minimum aspect ratio of 0.526[45]. Since we have an electric field stronger than the predicted critical value for a stationary drop, this demonstrates the stabilizing effect of the gravitational force.

The contaminated drop with an electric field is shown in Figure 5b. For this drop, the terminal velocity has increased to $V_T = 1.09 \times 10^{-2}\,\mathrm{m/s}$ compared to the contaminated drop without an electric field. This increase in terminal velocity is much larger than for the clean drop, which is caused by the lower average surface tension yielding a higher degree of stretching. An aspect ratio of 0.700 is calculated for the contaminated drop compared to 0.770 for the clean drop.

Finally, we observe that the electric field lines are close to perpendicular to the interface at the drop interface, and that the electric field magnitude is close to zero inside the drop. This indicates that our method of approximating a conductive drop in a dielectric medium by simulating a dielectric/dielectric system with high permittivity ratio is satisfactory.

3.3 Falling drop at high Reynolds number

We now consider a drop at a relatively high Reynolds number. We use the same parameters as above, with the exception of a higher radius, $R = 5.15 \times 10^{-3}$, and a lower matrix viscosity, $\mu_2 = 0.19$, to achieve a higher Reynolds number. The dimensionless parameters for this case becomes $\mathrm{Eo} = 6.4$ and $\mathrm{Mo} = 1.03 \times 10^{-5}$. For a clean drop, the calculated terminal velocity was $V_T = 0.131\,\mathrm{m/s}$ which gives $\mathrm{Re} = 67.4$. An experiment performed with the same parameters gave $\mathrm{Re} = 67.9$[33], which very close to the simulated value. Since the viscosity of the matrix fluid is lower in this case, we expect the boundaries

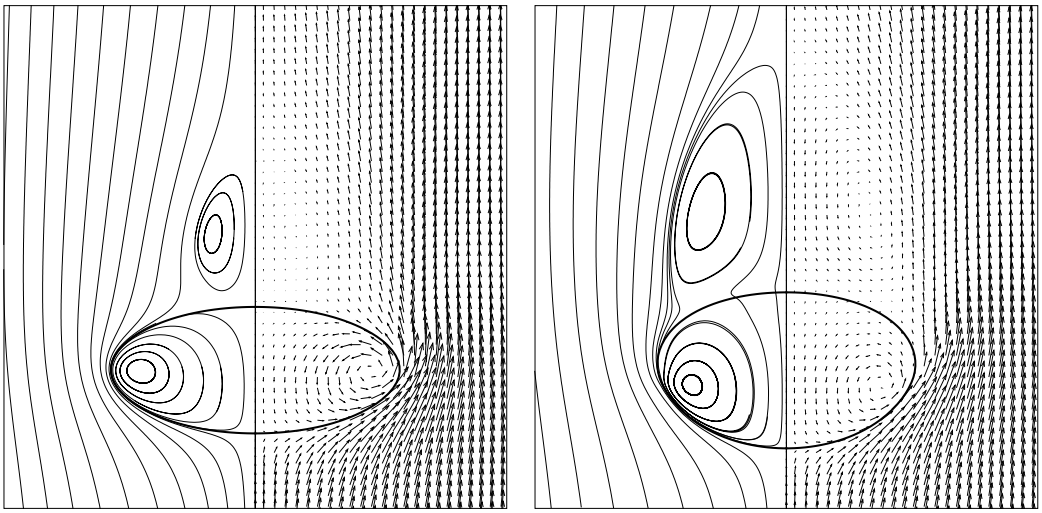

(a) Clean (b) Contaminated

Figure 6: High Re drop. Streamlines and velocity vectors in a coordinate system moving with the drop centroid. Velocity vectors are plotted at every other grid point.

to have less influence for this drop. The excellent agreement with the experiment indicates that this is indeed the case. Figure 6a shows the drop shape and velocity pattern. At this higher Re, the drop deforms into an ellipsoidal shape, and a vortex is formed behind the drop.

We then add surfactants to the system. It is well known that for contaminated drops or bubbles moving at higher Reynolds numbers through an otherwise stagnant fluid, the surfactants will be swept to the rear of the drop. This will create a region where the interface is nearly immobile due to the resulting high Marangoni stresses, while the front of the drop will be surfactant-free and mobile. The immobile region is often denoted the *stagnant cap*. Several models have been developed which relate the cap angle to e.g. the drag coefficient. The numerical method used here requires no assumption of a stagnant cap, and no *a priori* estimate of the cap angle is necessary.

The resulting drop shape and velocity pattern for the contaminated drop is given in Figure 6b. It is evident that the deformation is smaller than for the clean drop. Additionally, we see that the center of the internal vortex has moved closer to the front, and that the trailing vortex is larger for the contaminated drop. This results in a lower terminal velocity of $V_T = 0.119\,\mathrm{m/s}$ compared to $V_T = 0.131\,\mathrm{m/s}$ for the clean drop. This is a much lower difference than for the low Re drop.

The surfactant concentration is shown in Figure 7a. Here, the gradient in the surfactant concentration does not vary smoothly like for the low Re drop. Instead, there is no surfactant at the tip of the drop, followed by a sharp jump in concentration towards the back of the drop. This jump in concentration will effectively immobilize this part of the

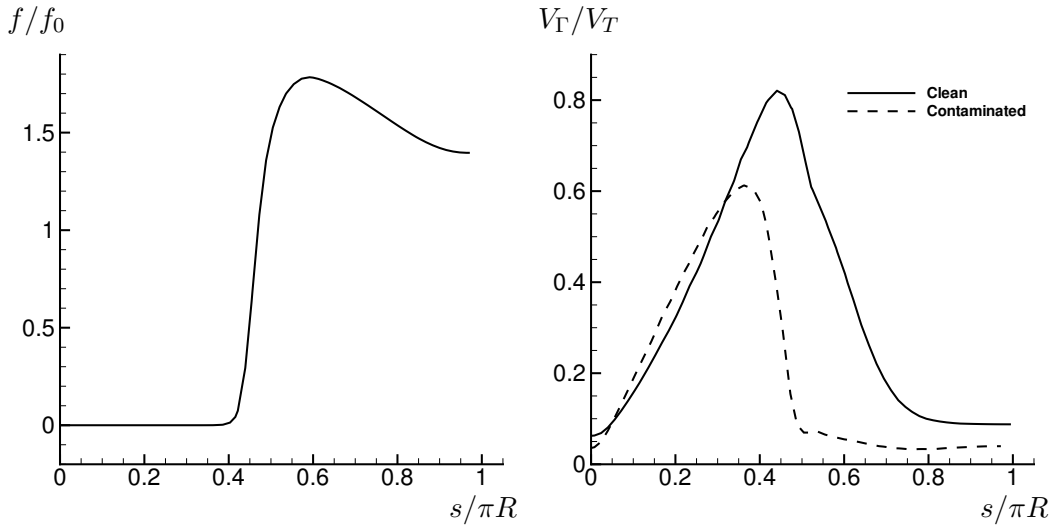

(a) Surfactant concentration (b) Interface velocities

Figure 7: High Re drop. Surfactant concentration and interface velocities as functions of arc length.

drop, due to high Marangoni stresses. This is further illustrated in Figure 7b, which shows the interface velocity for both the clean and contaminated drop. Here we clearly see that for the contaminated drop the interface velocity is greatly reduced in the region of high surfactant concentration.

We then consider the effect of an electric field. The electric capillary number is $\mathrm{Ca}_E = 0.7835$, which gives an electric field of $E_0 = 5 \times 10^5\,\mathrm{V/m}$. We use a higher Ca_E here since the stabilizing convection is stronger. For the clean drop, the terminal velocity increases to $V_T = 0.138\,\mathrm{m/s}$. As can be seen in Figure 8a, there is little change compared to the case without an electric field. For the contaminated drop, shown in Figure 8b, there is a more pronounced change. This is also reflected in the terminal velocity, which increases to the same as the clean drop, $V_T = 0.138\,\mathrm{m/s}$. Again, this is caused by the lower surface tension of the contaminated drop allowing a higher degree of stretching.

If the electric field is increased to $E_0 = 6 \times 10^5\,\mathrm{V/m}$, the clean drop remains stable, while the contaminated drop becomes unstable. This is due to the stagnant cap, which has a very low interfacial tension compared to the clean drop. This makes the drop less resistant to the electric stresses and renders it unstable at a lower electric field strength. The evolution of the drop is shown in Figure 9, with the drop revolved around the z-axis and colored according to the surfactant concentration. When the electric field is switched on, the back of the drop starts to stretch, while the front of the drop remains stable. Eventually, the stretched part develops a pointed tip and we see the formation of a small drop on the tip. It has been shown both experimentally and numerically that conductive drops become pointed and starts emitting small drops from the tips[45,40,27,6,42]. An

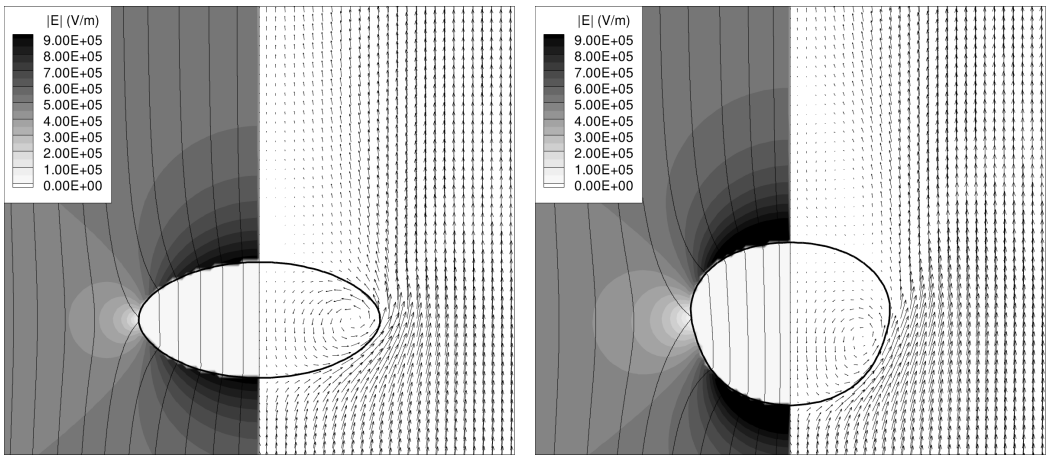

(a) Clean (b) Contaminated

Figure 8: High Re drop with electric field. The left part of the drop shows streamlines of the electric field and contours colored by the electric field magnitude. The right part of the drop shows velocity vectors in a coordinate system moving with the drop centroid. Velocity vectors are plotted at every other grid point.

interesting observation is that as the tip starts to form, surfactant is swept from the tip and towards the middle of the drop. The drop formed at the tip has a very low concentration of surfactants. This is a fundamentally different process from surfactant-covered drops being stretched in extensional flows or shear flows. For these flows, surfactant is swept to the drop tips and contributes to the tip-streaming process[32,5,39,47]. This creates small drops with high surfactant concentrations which consequently are very stable. The present simulations suggest that this is not the case for drops broken due to electric fields.

Another interesting phenomenon suggested by the experimental results of Ha & Yang[10] is that the presence of a surfactant can cause the break-up mode to change from bulbous end formation to tip-streaming. The proposed physical mechanism was the same as for drops in shear flows. Again, our numerical results suggest that this may not be the correct explanation for the observed behavior.

4 CONCLUSIONS

A level-set method for computations of interfacial flows with insoluble surfactants and electric fields was presented. It was shown that the method is more accurate than the standard level-set method at handling the pressure jump at the interface. Currently, the method only handles insoluble surfactants. A natural extension of the method is to include solubility. For instance, the method proposed in Teigen et al.[46] for the phase-field method is also applicable to the level-set method.

The method was used to study an axisymmetric drop falling in an otherwise quiescent fluid. It was found that the surfactant reduced the deformation and the terminal velocity

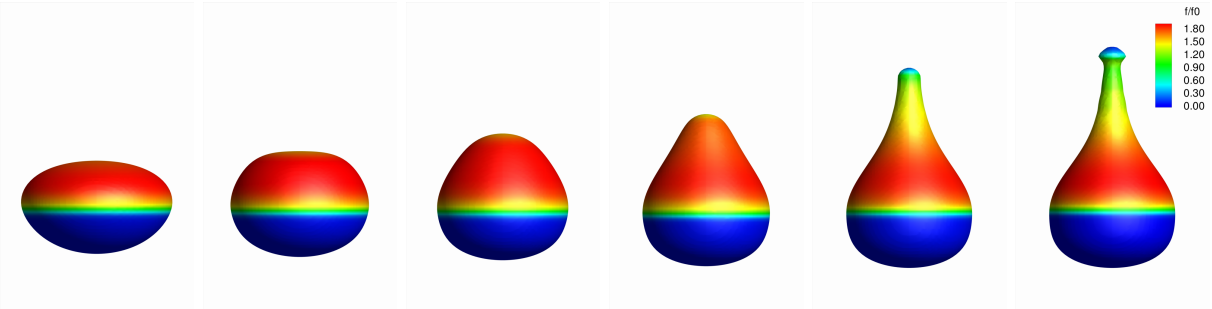

Figure 9: Behavior of contaminated drop above the critical field strength. The drop surface is colored according to surfactant concentration. The first frame shows the drop before the electric field is switched on. The subsequent frames are at times 0.7, 1.0, 1.3, 1.6 and 1.7 seconds after the field has been switched on.

of the drop. The reduction was most pronounced at low Reynolds number, where the drop remains spherical. Here, the surfactant-covered drop behaved similarly to a solid sphere. These results are in agreement with experiments and simulations in the literature. The effect of an electric field was mainly to increase the terminal velocity. This is due to the drop stretching in the direction of the electric field, which gives a lower projected interface area and hence lower drag. This effect was also more evident at lower Reynolds numbers, which was attributed to lower convection forces which allowed the drop to stretch more. The effect of an electric field on the contaminated drop was also to increase the terminal velocity. However, the effect was slightly higher here, due to the overall lower interfacial tension of the contaminated drop which gives a lower resistance to deformation.

Only two different drops were investigated in this study, and the surfactant parameters and electric fields were not varied. It would be instructive to investigate a wider range of drop shapes, and study the influence of the surfactant parameters and electric fields in more detail. In particular, the observed behavior of an unstable drop is fundamentally different from previous results for drops in extensional flows or shear flows, and this warrants further studies.

Acknowledgement

This work forms part of the Electrocoalescence project, supported by The Research Council of Norway (169466/S30), and by the following industrial partners: Aker Solutions AS, BP Exploration Operating Company Ltd, Hamworthy Technology and Products AS, Shell Technology Norway AS, Petrobras, Saudi Aramco and Statoil ASA.

References

[1] D. Adalsteinsson and J.A. Sethian. The fast construction of extension velocities in level set methods. *J. Comput. Phys.*, 148:2–22, 1999.

[2] S. Adami, X.Y. Hu, and N.A. Adams. A conservative SPH method for surfactant dynamics. *J. Comput. Phys.*, 229(5):1909 – 1926, 2010.

[3] E. Bjørklund. The level-set method applied to droplet dynamics in the presence of an electric field. *Comput. Fluids*, 38(2):358–369, 2008.

[4] R. Clift, J. R. Grace, and M. E. Weber. *Bubbles, Drops and Particles*. Dover, Mineola, 2005.

[5] R. A. De Bruijn. Tipstreaming of drops in simple shear flows. *Chem. Eng. Sci.*, 48:277–284, 1993.

[6] N. Dubash and A. J. Mestel. Breakup behavior of a conducting drop suspended in a viscous fluid subject to an electric field. *Phys. Fluids*, 19:072101, 2007.

[7] D. Enright, R. Fedkiw, J. Ferziger, and I. Mitchell. A hybrid particle level set method for improved interface capturing. *J. Comput. Phys.*, 183:83–116, 2002.

[8] J. S. Eow and M. Ghadiri. Electrostatic enhancement of coalescence of water droplets in oil: a review of the technology. *Chem. Eng. J.*, 85:357–368, 2002.

[9] R. P. Fedkiw. A non-oscillatory Eulerian approach to interfaces in multimaterial flows. *J. Comput. Phys.*, 152:457–492, 1999.

[10] J. Ha and S. Yang. Effect of nonionic surfactant on the deformation and breakup of a drop in an electric field. *J. Colloid and Interface Sci.*, 206(1):195 – 204, 1998.

[11] J. S. Hadamard. Mouvement permanent lent d'une sphère liquide et visqueuse dans un liquide visqueux. *CR Acad. Sci.*, 1911.

[12] M. Hameed, M. Siegel, Y.-N. Young, J. Li, M. R. Booty, and D. T. Papageorgiou. Influence of insoluble surfactant on the deformation and breakup of a bubble or thread in a viscous fluid. *J. of Fluid Mech.*, 594:307–340, 2008.

[13] E. B. Hansen. *Numerical simulation of droplet dynamics in the presence of an electric field*. PhD thesis, Norwegian University of Science and Technology, Trondheim, 2005.

[14] A. Hirsa and W. W. Willmarth. Measurements of vortex pair interaction with a clean or contaminated free surface. *J. Fluid Mech.*, 259:25–45, 1994.

[15] Y. T. Hu, D. J. Pine, and L. Gary Leal. Drop deformation, breakup, and coalescence with compatibilizer. *Phys. Fluids*, 12:484–489, 2000.

[16] J. Hua, L. K. Lim, and C. Wang. Numerical simulation of deformation/motion of a drop suspended in viscous liquids under influence of steady electric fields. *Phys. Fluids*, 20(11):113302, 2008.

[17] Steven D. Hudson, Alex M. Jamieson, and Brian E. Burkhart. The effect of surfactant on the efficiency of shear-induced drop coalescence. *J. Colloid Interface Sci.*, 265:409 – 421, 2003.

[18] Ashley J. James and John Lowengrub. A surfactant-conserving volume-of-fluid method for interfacial flows with insoluble surfactant. *J. of Comput. Phys.*, 201:685 – 722, 2004.

[19] Y. J. Jan. *Computational Studies of Bubble Dynamics*. PhD thesis, University of Michigan, 1994.

[20] G. S. Jiang and D. Peng. Weighted ENO schemes for Hamilton-Jacobi equations. *SIAM J. Sci. Comp.*, 21:2126–2143, 2000.

[21] M. Kang, R. Fedkiw, and X. Liu. A boundary condition capturing method for multiphase incompressible flow. *J. Sci. Comput.*, 15:323–360, 2000.

[22] D. I. Ketcheson and A. C. Robinson. On the practical importance of the SSP property for Runge-Kutta time integrators for some common Godunov-type schemes. *Int. J. Numer. Meth. Fluids*, 48(3):271–303, January 2005.

[23] J. F. B. M Kraaijevanger. Contractivity of Runge-Kutta methods. *BIT*, 31(3):482–528, 1991.

[24] E. Lac and G. M. Homsy. Axisymmetric deformation and stability of a viscous drop in a steady electric field. *J. Fluid Mech.*, 590:239–264, 2007.

[25] L. G. Leal. Flow induced coalescence of drops in a viscous fluid. *Phys. of Fluids*, 16(6):1833–1851, 2004.

[26] R. J. LeVeque and Z. L. Li. The immersed interface method for elliptic equations with discontinuous coefficients and singular sources. *SIAM J. Num. Anal.*, 31:1019–1044, 1997.

[27] L. E. Lundgaard, G. Berg, A. Pedersen, and P. J. Nilsen. Electrocoalescence of water drop pairs in oil. In *Proceedings of 14th International Conference on Dielectric Liquids (ICDL 2002)*, 2002.

[28] E. Marchandise, J. F. Remacle, and N. Chevaugeon. A quadrature-free discontinuous galerkin method for the level set equation. *J. Comput. Phys.*, 212:338 – 357, 2006.

[29] O. K. Matar and S. M. Troian. The development of transient fingering patterns during the spreading of surfactant coated films. *Phys. Fluids*, 11:3232–3246, 1999.

[30] J. R. Melcher and G. I. Taylor. Electrohydrodynamics: A review of the role of interfacial shear stresses. *Annu. Rev. Fluid Mech.*, 1:111–146, 1969.

[31] W. J. Milliken and L. G. Leal. The influence of surfactant on the deformation and breakup of a viscous drop - the effect of surfactant solubility. *J. Colloid and Interface Sci.*, 166:275–285, 1994.

[32] W. J. Milliken, H. A. Stone, and L. G. Leal. The effect of surfactant on transient motion of Newtonian drops. *Phys. Fluids A*, 5:69–79, 1993.

[33] Z. Mohamed-Kassim and E. K. Longmire. Drop coalescence through a liquid/liquid interface. *Physics of Fluids*, 16(7):2170–2181, 2004.

[34] M. Muradoglu and G. Tryggvason. A front-tracking method for computation of interfacial flows with soluble surfactants. *J. Comput. Phys.*, 227:2238–2262, 2008.

[35] E. Olsson and G. Kreiss. A conservative level set method for two phase flow. *J. Comput. Phys.*, 210(1):225–246, 2005.

[36] S. Osher and R. Fedkiw. *Level set methods and dynamic implicit surfaces*. Springer, 2003.

[37] Y. Pawar and K. J. Stebe. Marangoni effects on drop deformation in an extensional flow: The role of surfactant physical chemistry. I. insoluble surfactants. *Physics of Fluids*, 8(7):1738–1751, 1996.

[38] D. A. Di Pietro, S. Lo Forte, and N. Parolini. Mass preserving finite element implementations of the level set method. *Appl. Numer. Math.*, 56:1179–1195, 2006.

[39] Y. Y. Renardy, M. Renardy, and V. Cristini. A new volume-of-fluid formulation for surfactants and simulations of drop deformation under shear at a low viscosity ratio. *European Journal of Mechanics - B/Fluids*, 21:49 – 59, 2002.

[40] J. D. Sherwood. Breakup of fluid droplets in electric and magnetic fields. *J. Fluid Mech.*, 188:133 – 146, 1988.

[41] H. A. Stone and L. G. Leal. The effect of surfactants on drop deformation and breakup. *J. Fluid Mech*, 220:161–186, 1990.

[42] G. Supeene, C. R. Koch, and S. Bhattacharjee. Deformation of a droplet in an electric field: Nonlinear transient response in perfect and leaky dielectric media. *J. of Colloid and Interface Sci.*, 318(2):463 – 476, 2008.

[43] M. Sussman and E. Puckett. A coupled level set and volume-of-fluid method for computing 3D and axisymmetric incompressible two-phase flows. *J. Comput. Phys.*, 162:301–337, 2000.

[44] M. Sussman, P. Smereka, and S. Osher. A level set approach for computing solutions to incompressible two-phase flow. *J. Comput. Phys.*, 114:146–159, 1994.

[45] G. Taylor. Disintegration of water droplets in an electric field. *Proc. R. Soc. London*, 280:383–397, 1964.

[46] K. E. Teigen, X. Li, J. Lowengrub, F. Wang, and A. Voigt. A diffuse-interface approach for modelling transport, diffusion and adsorption/desorption of material quantities on a deformable interface. *Comm. Math. Sci.*, 7:1009–1037, 2009.

[47] K. E. Teigen, J. Lowengrub, P. Song, , and A. Voigt. A diffuse-interface method for two-phase flows with soluble surfactants. *J. Comput. Phys.*, 2009. Submitted.

[48] G. Tomar, D. Gerlach, G. Biswas, N. Alleborn, A. Sharma, F. Durst, S. W. J. Welch, and A. Delgado. Two-phase electrohydrodynamic simulations using a volume-of-fluid approach. *J. Comput. Phys.*, 227:1267–1285, 2007.

[49] S. M. Troian, E. Herbolzheimer, and S. A. Safran. Model for the fingering instability of spreading surfactant drops. *Phys. Rev. Lett.*, 65:333–336, Jul 1990.

[50] G. Tryggvason, J. Abdollahi-Alibeik, W. W. Willmarth, and A. Hirsa. Collision of a vortex pair with a contaminated free surface. *Phys. Fluids A*, 4:1215–1229, 1992.

[51] S. P. van der Pijl, A. Segal, C. Vuik, and P. Wesseling. A mass-conserving level-set method for modelling of multi-phase flows. *Int. J. Num. Meth. Fluids*, 47:339–361, 2005.

[52] S. W. J. Welch and G. Biswas. Direct simulation of film boiling including electrohydrodynamic forces. *Phys. Fluids*, 19(012106), 2007.

[53] J. J. Xu, Z. Li, J. Lowengrub, and H. Zhao. A level set method for interfacial flows with surfactant. *J. Comput. Phys.*, 212:590–616, 2006.

[54] J. J. Xu and H. Zhao. An Eulerian formulation for solving partial differential equations along a moving interface. *J. Sci. Comp.*, 19:573–594, 2003.

[55] N. O. Young, J. S. Goldstein, and M. J. Block. The motion of bubbles in a vertical temperature gradient. *J. Fluid Mech.*, 6(03):350–356, 1959.

[56] J. Zhang, D.M. Eckmann, and P.S. Ayyaswamy. A front tracking method for a deformable intravascular bubble in a tube with soluble surfactant transport. *J. Comput. Phys.*, 214:366 – 396, 2006.

[57] J. Zhang and D. Y. Kwok. A 2D lattice Boltzmann study on electrohydrodynamic drop deformation with the leaky dielectric theory. *J. Comput. Phys.*, 206:150–161, 2005.

[58] H. K. Zhao, T. Chan, B. Merriman, and S. Osher. A variational level set approach to multiphase motion. *J. Comput. Phys.*, 127(1):179 – 195, 1996.